

Effective theory of rotationally faulted multilayer graphene - the local limit

M. Kindermann and P. N. First

School of Physics, Georgia Institute of Technology, Atlanta, Georgia 30332, USA

(Dated: November 29, 2018)

Interlayer coupling in rotationally faulted graphene multilayers breaks the local sublattice-symmetry of the individual layers. Earlier we have presented a theory of this mechanism, which reduces to an effective Dirac model with space-dependent mass in an important limit. It thus makes a wealth of existing knowledge available for the study of rotationally faulted graphene multilayers. Agreement of this theory with a recent experiment in a strong magnetic field was demonstrated. Here we explore some of the predictions of this theory for the system in zero magnetic field at large interlayer bias, when it becomes local in space. We use that theory to illuminate the physics of localization and velocity renormalization in twisted graphene bilayers.

PACS numbers: 73.20.-r, 73.21.Cd, 73.22.Pr

I. INTRODUCTION

Experiments indicate that the 10–100 individual graphene layers grown on the carbon-terminated face of SiC are surprisingly well decoupled from one another electronically. Early spectroscopic measurements^{1,2} found a linear low-energy electronic dispersion to the experimental precision, like that of single-layer graphene^{3,4}. In scanning tunneling microscopy/spectroscopy (STM/STS) measurements the Landau level quantization of the material in a magnetic field was found to be essentially that of single-layer graphene⁵. Theoretically it has been shown that this approximate decoupling of different layers is due to a relative twist of the layers with respect to each other^{6–12}. A renormalization of the electron velocity^{7,11}, van Hove singularities¹³, and interlayer transport¹⁴ have been discussed as residual effects of the interlayer coupling.

In a recent STM measurement on multilayer epitaxial graphene¹⁵ a spatially modulated splitting $\Delta \lesssim 10$ meV of the zeroth Landau level (LL_0) was observed. In view of the above this finding is intriguing, since the states forming LL_0 of an isolated layer of graphene without electron-electron interactions are degenerate. Many aspects of the experimental data indicate that this splitting is due to the coupling between graphene layers. In Ref. 15 we proposed a phenomenological theory of the interlayer interaction. In that theory a “staggered” electric potential (a potential with opposite sign on the two sublattices) breaks the sublattice-symmetry locally. This model qualitatively accounts for the main features of the experimental data. In Ref. 16 we have presented a microscopic theory of the interlayer coupling in rotationally faulted graphene multilayers that reduces to the phenomenological model of Ref. 15 in certain limits. The theory is formulated for a single layer of graphene and it accounts for the coupling to other layers by effective potentials and an effective mass that are possibly non-local in space. The theory of Ref. 16 accounts for the main features of the experimental findings¹⁵, both qualitatively and quantitatively.

A number of intriguing results have been obtained

theoretically in electronic structure calculations of rotationally-faulted multilayer graphene also in zero magnetic field^{11,17}. One may therefore ask whether the theory of Ref. 16 can provide an intuitive understanding also of these results, as it did for the physics of the material in high magnetic field: is that theory an advantageous starting point to exploring the physics of rotationally-faulted multilayer graphene also in zero magnetic field?

In this article we give a partial answer to that question by exploring predictions of the theory of Ref. 16 in zero magnetic field for quantities that have displayed interesting features in the calculations of Ref. 11 and by seeking an interpretation of the results in qualitative terms. We focus on the spatially local limit of the theory 16 that corresponds to the phenomenological model of Ref. 15: a single-layer Dirac model with oscillating effective potentials and a space-dependent mass. That limit is realized in the presence of a large interlayer bias. The theory predicts a density of states in qualitative agreement with experimental topographic STM measurements. Moreover, our calculation qualitatively reproduces some of the main observations of the mentioned electronic structure calculations of twisted graphene bilayers¹¹ such as a localization of electronic states and a corresponding velocity suppression. The agreement is not quantitative, since the calculations of Ref. 11 were not obtained in the spatially local limit assumed here. But in the framework of the theory of Ref. 16 these predictions do have an intuitive explanation in terms of known results about the Dirac equation with a space-dependent mass. This suggests that this theory is indeed an advantageous starting point for the exploration of the physics of rotationally faulted graphene multilayers also in zero magnetic field.

We start our discussion with Section II, where we restate the model on which our earlier theory¹⁶ is based. In Section III we take the limit of a large interlayer bias, when the effective theory of Ref. 16 becomes local in space. We then proceed to evaluate the density of states and the electron velocity renormalization predicted by this theory in zero magnetic field. We do that first perturbatively in the interlayer coupling in Section IV. In Section V we then analyze nonperturbatively a toy model

that resembles the original theory, but assumes a simplified spatial structure of the effective staggered potential. We conclude in Section VI.

II. MODEL

In this Section we recall the model of Ref. 16, which underlies also the present article. We analyze the electron dynamics in a graphene layer “0” when coupled to a second layer “1,” twisted by a relative angle θ ($\theta = 0^\circ$ for aligned honeycomb lattices, *cf.* Fig. 1), neglecting electron-electron interactions. The corresponding dynamics in multilayers at perturbatively weak interlayer coupling, such as in the experiment¹⁵, are obtained by summation over all layers coupled to the top layer 0. Twisted graphene bilayers have been described before^{7,9–12} by a tight-binding model with a local interlayer coupling Hamiltonian that has parameters fitted to experiment¹⁸,

$$H_{\text{int}} = \int d\mathbf{r} \Psi^{(0)\dagger}(\mathbf{r}) \Gamma(\mathbf{r}) \Psi^{(1)}(\mathbf{r}) + h.c. \quad (1)$$

Here, the spinors $\Psi^{(j)}$ collect the amplitudes for electrons on the two sublattices of layer $j \in \{0, 1\}$. The interlayer coupling Γ has contributions at wavevectors $\mathbf{b}^{(0)} - \mathbf{b}^{(1)}$, where $\mathbf{b}^{(j)}$ are reciprocal vectors of the graphene lattice in layer j ¹². The Fourier components of Γ quickly decay with increasing wavevector^{9,10,12}. We therefore neglect all but the zero wavevector component, setting $\Gamma(\mathbf{r}) = \gamma$. In the “first star approximation” of the wavefunctions employed below, the distinction between commensurate and incommensurate interlayer rotations then disappears. This approximation is valid for energies $\varepsilon \gg \mathcal{V}$, where \mathcal{V} is set by the Fourier components of Γ that directly connect K-points of the two layers¹². We take the limit $0 < \theta \ll 1$, when $\mathcal{V} \ll \gamma$ (in the experiment¹⁵ $\theta \approx 0.25^\circ$ and according to the estimate $\mathcal{V} \simeq \theta^2 \gamma$ of Ref. 12 this approximation is justified at all accessed energies).

In our limit $0 < \theta \ll 1$ a long-wavelength description is appropriate, where the isolated layers j are described by Dirac model Hamiltonians (we set $\hbar = 1$)

$$H^{(j)} = v \int d\mathbf{r} \sum_{\nu} \psi_{\nu}^{(j)\dagger}(\mathbf{r}) [\boldsymbol{\sigma}_{\nu} \cdot (-i\nabla + e\mathbf{A}(\mathbf{r}))] \psi_{\nu}^{(j)}(\mathbf{r}). \quad (2)$$

Here, $\boldsymbol{\sigma}_{\nu} = (\nu\sigma_x, \sigma_y)$ is a vector of Pauli matrices, $\nu = \pm$ is the valley spin, $-e$ the electron charge, and v the electron velocity in graphene. We have included an external vector potential \mathbf{A} to describe a perpendicular magnetic field B . Eq. (2) acts on the long-wavelength spinors $\psi_{\mu\nu}^{(j)}$ defined by $\Psi_{\mu}^{(j)}(\mathbf{r}) = \sum_{\nu} u_{\mu\nu}^{(j)}(\mathbf{r}) \psi_{\mu\nu}^{(j)}(\mathbf{r})$. We write the Bloch functions $u_{\mu\nu}^{(j)}(\mathbf{r}) = \{\sum_p \exp[i\mathbf{K}_{p\nu}^{(j)} \cdot (\mathbf{r} - \boldsymbol{\tau}_{\mu}^{(j)})]\} / \sqrt{3}$ in the “first star approximation” appropriate for the interlayer coupling problem¹². Here, p sums over the three equivalent Brillouin zone corners $\mathbf{K}_{p\nu}^{(j)}$ that form the

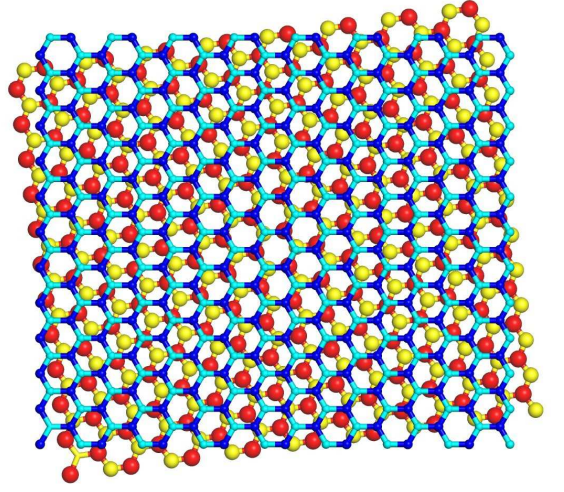


FIG. 1: (color online) Moiré pattern created by two graphene lattices with a relative twist. Top layer A/B sublattice atoms are shown as small blue/cyan (dark/light) spheres and connectors; bottom layer A/B atoms are shown as large red/yellow (dark/light) spheres. A region of AA alignment lies at the center, where each top-layer atom has a neighbor in the bottom layer. The AA region is surrounded by three AB- and three BA-aligned regions where atoms on only one top-layer sublattice have direct neighbors in the bottom layer. As a consequence, the sublattice-symmetry is broken locally.

Dirac point of valley ν ¹² and $\boldsymbol{\tau}_{\mu}^{(j)}$ gives the position of an atom on sublattice $\mu \in \{A, B\}$ within the unit cell of layer j . In the long-wavelength theory (which neglects inter-valley processes) the interlayer coupling reads

$$H_{\text{int}} = \int d\mathbf{r} \sum_{\nu} \psi_{\nu}^{(0)\dagger}(\mathbf{r}) t_{\nu}(\mathbf{r}) \psi_{\nu}^{(1)}(\mathbf{r}) + h.c., \quad (3)$$

with a matrix t whose long-wavelength components have wavevectors $\delta\mathbf{K}_{p\nu} = (R_{\theta} - 1)\mathbf{K}_{p\nu}^{(0)}$. Here, R_{θ} is a rotation around the z -axis by angle θ . Retaining only those long-wavelength parts of t we find

$$t_{\nu}^{\mu\mu'}(\mathbf{r}) = \frac{\gamma}{3} \sum_p e^{i\delta\mathbf{K}_{p\nu} \cdot \mathbf{r} + i\mathbf{K}_{p\nu} \cdot (\boldsymbol{\tau}_{\mu}^{(0)} - \boldsymbol{\tau}_{\mu'}^{(1)})}, \quad (4)$$

where terms of order θ are neglected, while terms of order θKr are kept as they may grow large.

III. EFFECTIVE THEORY

We next integrate out layer $j = 1$ in order to arrive at an effective Hamiltonian $H_0^{\text{eff}}(\omega) = H_0 + \delta H_0^{\text{eff}}(\omega)$ for the top layer $j = 0$, with

$$\delta H_0^{\text{eff}}(\omega) = H_{\text{int}}(\omega + V - H_1)^{-1} H_{\text{int}}. \quad (5)$$

We include an interlayer bias V that accounts for different doping levels of the two layers²⁷. In general, H_0^{eff} is nonlocal in space and it depends on the energy ω . In the

limit of a large interlayer bias, however, $|V| \gg \omega, \gamma, \theta v/a$, the sum $\omega + V - H_1$ becomes momentum- and energy-independent to a good approximation. The spatial non-locality and the energy-dependence of H_0^{eff} then may be neglected and H_0^{eff} becomes a conventional Dirac Hamiltonian (2) with a matrix potential

$$\delta H_0^{\text{eff}} = \int d\mathbf{r} \sum_{\nu} \psi_{\nu}^{(0)\dagger}(\mathbf{r}) \frac{t_{\nu}(\mathbf{r}) t_{\nu}^{\dagger}(\mathbf{r})}{V} \psi_{\nu}^{(0)}(\mathbf{r}), \quad (6)$$

which we parametrize as

$$\frac{t_{\nu}(\mathbf{r}) t_{\nu}^{\dagger}(\mathbf{r})}{V} = V^{\text{eff}}(\mathbf{r}) + \nu v e \sigma_{\nu} \cdot \mathbf{A}^{\text{eff}}(\mathbf{r}) + m^{\text{eff}}(\mathbf{r}) v^2 \sigma_z. \quad (7)$$

The interlayer coupling in this limit generates effective scalar and vector potentials V^{eff} and \mathbf{A}^{eff} , respectively, and a mass term $\propto \sigma_z m^{\text{eff}} v^2$ that implies an effective staggered potential $V_{AB}^{\text{eff}} = m^{\text{eff}} v^2$ in locally Bernal stacked regions. It follows from Eq. (4) that $\delta H_{0\nu}^{\text{eff}}$ oscillates in space with wavevectors $\mathbf{G} = (R_{\theta} - 1)\mathbf{b}$, where \mathbf{b} is in the “first star” of reciprocal lattice vectors of graphene. We plot $\delta H_{0\nu}^{\text{eff}}$ in the parameterization of Eq.

(7) in Fig. 2. The effective Hamiltonian (6) promises rich physics. In particular the effective mass term is expected to have profound implications such as topologically confined states^{19,20}. In Ref. 16 we have shown that the above effective theory qualitatively and quantitatively accounts for many features of the experiment¹⁵, which was done in a strong magnetic field. In the remainder of this article we explore some of the consequences of the effective potentials (7) in zero magnetic field.

IV. PERTURBATIVE RESULTS

We first explore the perturbative limit of weak interlayer coupling $\gamma^2 \ll V v \delta K$ with correspondingly weak effective potentials, Eq. (7). To this end we do perturbation theory in δH_0^{eff} . We first obtain the perturbative corrections to the low-energy density of states $\rho_0(\mathbf{r}) = \lim_{\varepsilon \rightarrow 0} \rho(\mathbf{r}, \varepsilon)/\varepsilon$, as probed in STM measurements. The lowest order correction to $\rho_0(\mathbf{r}) = \lim_{\varepsilon \rightarrow 0} \rho(\mathbf{r}, \varepsilon)/\varepsilon$ vanishes. The leading spatially varying contribution appears at second order in δH_0^{eff} :

$$\begin{aligned} \delta \rho_0(\mathbf{r}) = & \frac{1}{2\pi v^2} \int \frac{d\varphi_k}{2\pi} \sum_{\mathbf{G}, \mathbf{G}' \neq 0, \mathbf{G} \neq \mathbf{G}', s', s''} \lim_{|\mathbf{k}| \rightarrow 0} \left[\frac{\langle s, \mathbf{k}, \nu | \delta H_{0\nu}^{\text{eff}} | s'', \mathbf{G}', \nu \rangle \langle s'', \mathbf{G}', \nu | \mathbf{r} \rangle \langle \mathbf{r} | s', \mathbf{G}, \nu \rangle \langle s', \mathbf{G}, \nu | \delta H_{0\nu}^{\text{eff}} | s, \mathbf{k}, \nu \rangle}{v^2 |\mathbf{G}| |\mathbf{G}'|} \right. \\ & \left. + 2 \text{Re} \frac{\langle s, \mathbf{k}, \nu | \mathbf{r} \rangle \langle \mathbf{r} | s'', \mathbf{G} - \mathbf{G}', \nu \rangle \langle s'', \mathbf{G} - \mathbf{G}', \nu | \delta H_{0\nu}^{\text{eff}} | s', \mathbf{G}, \nu \rangle \langle s', \mathbf{G}, \nu | \delta H_{0\nu}^{\text{eff}} | s, \mathbf{k}, \nu \rangle}{v^2 |\mathbf{G}| |\mathbf{G} - \mathbf{G}'|} \right]. \end{aligned} \quad (8)$$

Here, $|s, \mathbf{k}, \nu\rangle$ is an eigenstate of Eq. (2) at $\mathbf{A} = 0$ with wavevector \mathbf{k} and energy $sv|\mathbf{k}|$ in valley ν ,

$$\langle \mathbf{r} | s, \mathbf{k}, \nu \rangle = \frac{1}{\sqrt{2}} e^{i\mathbf{k} \cdot \mathbf{r}} \begin{pmatrix} 1 \\ i s \nu e^{i\nu \varphi_k} \end{pmatrix}, \quad (9)$$

where $\varphi_k = \arctan(k_y/k_x)$. The sums over wavevectors \mathbf{G}, \mathbf{G}' in Eq. (8) runs over all wavevectors contributing to δH_0^{eff} . Eq. (8) evaluated for the effective Hamiltonian (6) results in

$$\delta \rho_0(\mathbf{r}) = \sum_{\mathbf{G}, \mathbf{G}' \neq 0, \mathbf{G} \neq \mathbf{G}'} e^{i(\mathbf{G} - \mathbf{G}') \cdot \mathbf{r}} [V^{\text{eff}*}(\mathbf{G}) V^{\text{eff}}(\mathbf{G}') + m^{\text{eff}*}(\mathbf{G}) m^{\text{eff}}(\mathbf{G}') + \mathbf{A}^{\text{eff}*}(\mathbf{G}) \cdot \mathbf{A}^{\text{eff}}(\mathbf{G}')] \frac{1 + (|\mathbf{G}| + |\mathbf{G}'|)/|\mathbf{G} - \mathbf{G}'|}{2\pi v^4 |\mathbf{G}| |\mathbf{G}'|}. \quad (10)$$

We plot the resulting relative correction to the density of states $\delta \rho_0/\rho_0 = 2\pi v^2 \delta \rho_0$ in Fig. 3. The result compares well with the typical moiré patterns observed in STM topography. This suggests that density of states corrections due to the effective potentials Eq. (7) may be one of the mechanisms that generate these patterns, besides simple geometric height variations of the top graphene layer (which would be the most straight forward interpretation of topographic STM maps).

We next evaluate the perturbative correction to the electron velocity at the Dirac point in direction of the momentum $v_{\hat{\mathbf{k}}} = \lim_{k \rightarrow 0} \mathbf{v}(\mathbf{k}) \cdot \hat{\mathbf{k}}$, where $\hat{\mathbf{k}} = \mathbf{k}/|\mathbf{k}|$. One

has²¹

$$\delta v_{\hat{\mathbf{k}}} = \lim_{|\mathbf{k}| \rightarrow 0} \frac{d}{d|\mathbf{k}|} \sum_{s', \mathbf{G}} \frac{|\langle s, \mathbf{k}, \nu | \delta H_{0\nu}^{\text{eff}} | s', \mathbf{k} - \mathbf{G}, \nu \rangle|^2}{v(|\mathbf{k}| - s'|\mathbf{k} - \mathbf{G}|)}, \quad (11)$$

which, for our $\delta H_{0\nu}^{\text{eff}}$ evaluates to

$$\begin{aligned} \delta v_{\hat{\mathbf{k}}} = & -2v \sum_{\mathbf{G} \neq 0} \left\{ \frac{|V^{\text{eff}}(\mathbf{G})|^2 [|\mathbf{G}|^2 - (\hat{\mathbf{k}} \cdot \mathbf{G})^2]}{v^2 |\mathbf{G}|^4} \right. \\ & \left. + \frac{|m^{\text{eff}}(\mathbf{G})|^2 (\hat{\mathbf{k}} \cdot \mathbf{G})^2}{v^2 |\mathbf{G}|^4} \right\}. \end{aligned} \quad (12)$$

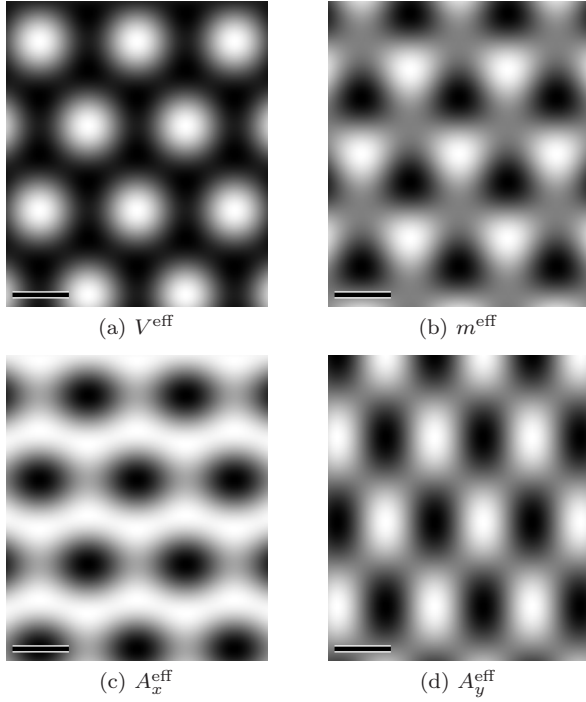


FIG. 2: (a) Effective potential V^{eff} , (b) effective mass m^{eff} , (c) A_x^{eff} , and (d) A_y^{eff} of Eq. (7) as functions of $\mathbf{r}\theta/a$ in grey-scale. Scale bars span a unity increment in $\mathbf{r}\theta/a$, where a is the C-C bond length (0.142 nm). Note the expected sixfold and threefold symmetries of V^{eff} and m^{eff} , respectively. \mathbf{A}^{eff} transforms as a vector under rotations.

Here, we have used that $\mathbf{G} \cdot \mathbf{A}(\mathbf{G}) = 0$, which holds in our approximations. We note that the effective mass suppresses the electron velocity as was found for an oscillating scalar potential $V(\mathbf{r})$ in Ref. 21. However, differently from a scalar potential, that velocity suppression is in the case of a mass not perpendicular to the direction \mathbf{G} along which m^{eff} varies, but along that direction. For the effective Hamiltonian (6) [with $\mathbf{b} = 0$ in Eq. (4)] Eq. (12) evaluates to

$$\delta v_{\mathbf{k}} = -\frac{|\gamma|^4 a^2}{24\pi^2 \theta^2 V^2}, \quad (13)$$

which is isotropic in space. We anticipate anisotropic contributions to $\delta v_{\mathbf{k}}$ at higher orders of perturbation theory. The interlayer coupling reduces the velocity, in agreement with earlier calculations^{7,11} for twisted bilayers at $V = 0$. We conclude that in the perturbative regime of weak interlayer coupling the predictions of our theory are consistent with earlier experimental and theoretical work. They moreover have a straightforward interpretation in terms of previous results for electrons in a superlattice potential²¹.

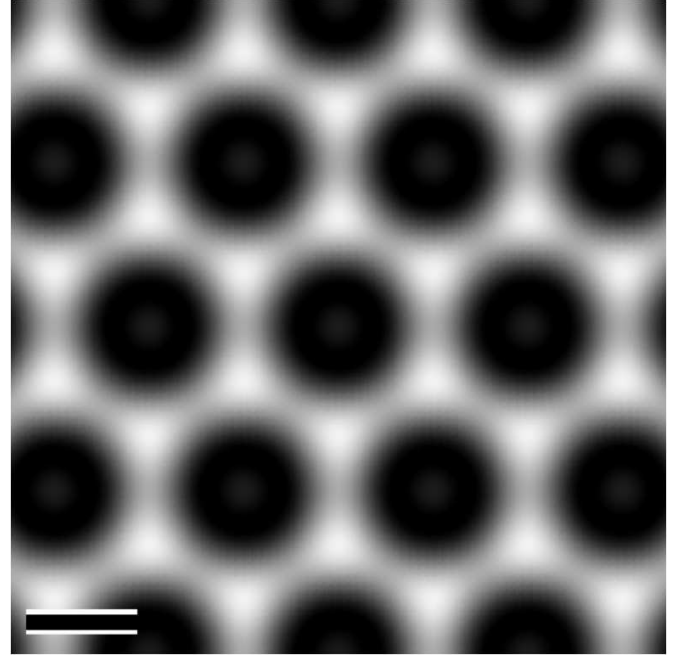


FIG. 3: Perturbative correction to the low-energy density of states ($\delta\rho_0/\rho_0$) due to δH_0^{eff} . The scale bar corresponds to one unit in $\mathbf{r}\theta/a$, where θ is the rotation angle between layers and a is the C-C bond length (0.142 nm). For a rotation angle of 3° , interlayer coupling of $\gamma = 300$ meV, and an interlayer bias of $V = 400$ meV (stretching the limits of our locality assumption) the image corresponds to a $16 \text{ nm} \times 16 \text{ nm}$ area with $\delta\rho_0/\rho_0$ ranging from -0.125 (black) to 0.125 (white).

V. NONPERTURBATIVE RESULTS

We now turn to the more challenging, but also more interesting nonperturbative limit. For strongly coupled, twisted graphene bilayers a number of intriguing results have been obtained in electronic structure calculations^{11,17}. For instance, a localization of the electronic wavefunctions in locally AA-stacked regions of the sample and a severe suppression of the electron velocity at small twist angles have been observed¹¹. Here, we show that the mentioned phenomena find an intuitive interpretation in terms of the oscillating mass in a toy model of our effective theory. In this toy model we assume translational invariance in one space direction. Our calculation extends earlier theory of Dirac electrons with a (scalar) superlattice potential²²⁻²⁴ to the case of a periodic mass term.

Our toy model has a mass term, which oscillates in only one space-direction:

$$m^{\text{eff}}(\mathbf{r}) = m \text{sgn}[\cos(x/l)]. \quad (14)$$

Although not directly applicable to the problem of the interlayer coupling in multilayer graphene, such a model is expected to capture some of the same physics. We add a term $m^{\text{eff}}v^2\sigma_z$ to Eq. (2) at $\mathbf{A} = 0$ and find the electronic spectrum along the lines of Ref. 24. The re-

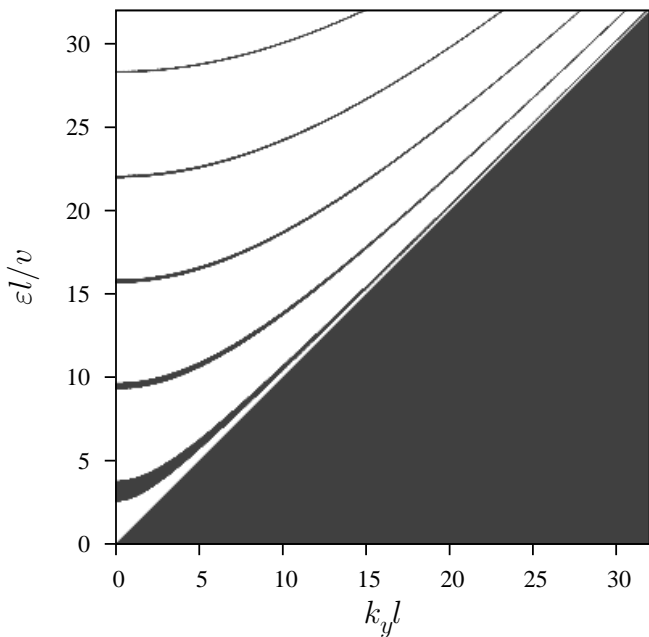


FIG. 4: Bandstructure of a Dirac model subject to a mass term Eq. (14) oscillating on a length scale l . In the plot, to every momentum k_y , the energies ε where electronic states exist are marked white. For the plot we chose $m = v/l$

sulting band structure as a function of the momentum k_y in the direction with translational invariance is plotted in Fig. 4. In presence of the periodic mass the electronic spectrum breaks up into minibands, as for periodic scalar potentials^{22,23}. Differently from the scalar case, however, we find that a periodic mass does not generate new Dirac points, even in the nonperturbative limit $vml \gg 1$. Instead, the bandwidth of the lowest energy band becomes exponentially suppressed in vml with correspondingly suppressed electron velocity: the velocity in x -direction at zero energy is exponentially small in vml ,

$$v_x|_{\varepsilon=0} = v \frac{vml}{\sqrt{2 \cosh vml - 2}}. \quad (15)$$

The wavefunctions at large vml have dominant weight around the locations $x = 2\pi n$ (with integer n) where m^{eff} changes sign. Those are the locations, where for an isolated kink of m^{eff} , i.e. a point at which m^{eff} changes sign, topologically protected zero energy states are expected^{19,20,25,26}. The lowest energy band observed in Fig. 4 may be thought of emerging from hybridization of those zero energy states. The larger vml the less overlap occurs between the states localized at adjacent kinks of m^{eff} . This qualitatively explains the exponentially small bandwidth of the lowest energy band in Fig. 4.

The above findings closely resemble the above-mentioned observations of earlier studies of twisted graphene bilayers¹¹. Also there the wavefunctions were reported to be localized in the AA-stacked regions of the moiré pattern when $\theta \ll 1$, which implies large l , with

$vml \gg 1$. Those are indeed the regions, where m^{eff} in H^{eff} , Eq. (7), changes sign. They thus directly correspond to the regions where the wavefunctions in our toy model Eq. (14) are concentrated. Moreover, in Ref. 11 the electron velocity was found to be strongly suppressed at small θ , corresponding to large vml . Also this is in qualitative agreement with the prediction of an exponential suppression of v_x by our model [Eq. (15)].

Although our theory is not directly applicable to the calculation of Ref. 11, because that calculation was done at $V = 0$ and the moiré pattern was naturally two-dimensional, it indeed appears to capture some of its essential physics. The above calculation thus suggests an intuitive interpretation of some of the prominent non-perturbative effects in twisted graphene bilayers in terms of zero energy states that are induced by the topology of the mass term in our model.

VI. CONCLUSIONS

In this article we have discussed some of the implications of the effective theory of rotationally-faulted multilayer graphene that was put forward in Ref. 16. We have focused on its local limit of a large interlayer bias, when this effective theory takes the form of a conventional Dirac model with space-dependent potentials and mass. While we discussed the implications of that theory for graphene multilayers in a magnetic field in Ref. 16, here we have explored its consequences in zero magnetic field. In the perturbative limit of weak interlayer coupling we found corrections to the density of states that are consistent with the typical moiré patterns observed in topographic STM measurements. This suggests that these patterns may not only arise because of height fluctuations, but may at least partially be due to density of states variations. We moreover have found a velocity correction consistent with earlier calculations in different limits.

To access the most interesting nonperturbative regime of strong interlayer coupling we have analyzed a toy model that captures most of the essential ingredients of our effective theory. We have demonstrated that that model predicts almost localized electronic states and an exponential velocity suppression. These predictions give an intuitive interpretation to prior electronic structure calculations for twisted graphene bilayers in terms of topologically protected zero energy states localized at kinks of an oscillatory Dirac mass term. Partially answering the question we raised at the outset, the presented calculations lead us to the following conclusion: while our real-space theory of the interlayer coupling certainly is an advantageous description of twisted graphene bilayers with a large interlayer bias, it qualitatively captures much of their essential physics even without such bias, when it does not strictly apply. The theory of Ref. 16 indeed appears to be an advantageous approach to the physics of twisted graphene bilayers, also in zero mag-

netic field.

Acknowledgments

We gratefully acknowledge discussions with W. de Heer, E. J. Mele, D. L. Miller. This work was funded

in part by the NSF (DMR-1106131 and DMR-0820382) and by the Semiconductor Research Corporation Nanoelectronics Research Initiative (NRI-INDEX).

-
- ¹ M. L. Sadowski, G. Martinez, M. Potemski, C. Berger, and W. A. de Heer, *Phys. Rev. Lett.* **97**, 266405 (2006).
 - ² M. Orlita, C. Faugeras, P. Plochocka, P. Neugebauer, G. Martinez, D. K. Maude, A.-L. Barra, M. Sprinkle, C. Berger, W. A. de Heer, et al., *Phys. Rev. Lett.* **101**, 267601 (2008).
 - ³ K. Novoselov, A. Geim, S. Morozov, D. Jiang, M. Katsnelson, I. Grigorieva, S. Dubonos, and A. Firsov, *Nature* **438**, 197 (2005).
 - ⁴ Y. Zhang, Y.-W. Tan, H. L. Stormer, and P. Kim, *Nature* **438**, 201 (2005).
 - ⁵ D. L. Miller, K. D. Kubista, G. M. Rutter, M. Ruan, W. A. de Heer, P. N. First, and J. A. Stroscio, *Science* **324**, 924 (2009).
 - ⁶ S. Latil, V. Meunier, and L. Henrard, *Phys. Rev. B* **76**, 201402 (2007).
 - ⁷ J. M. B. L. dos Santos, N. M. R. Peres, and A. H. C. Neto, *Phys. Rev. Lett.* **99**, 256802 (2007).
 - ⁸ J. Hass, F. Varchon, J. E. Millán-Otoya, M. Sprinkle, N. Sharma, W. A. de Heer, C. Berger, P. N. First, L. Magaud, and E. H. Conrad, *Phys. Rev. Lett.* **100**, 125504 (2008).
 - ⁹ S. Shallcross, S. Sharma, and O. A. Pankratov, *Phys. Rev. Lett.* **101**, 056803 (2008).
 - ¹⁰ S. Shallcross, S. Sharma, E. Kandelaki, and O. A. Pankratov, *Phys. Rev. B* **81**, 165105 (2010).
 - ¹¹ L. M. Guy Trambly de Laissardière, Didier Mayou, *Nano Lett.* **10**, 804 (2010).
 - ¹² E. J. Mele, *Phys. Rev. B* **81**, 161405 (2010).
 - ¹³ G. Li, A. Luican, J. M. B. L. dos Santos, A. H. C. Neto, A. Reina, J. Kong, and E. Andrei, *Nature Physics* **6**, 44 (2010).
 - ¹⁴ R. Bistritzer and A. H. MacDonald, *Phys. Rev. B* **81**, 245412 (2010).
 - ¹⁵ D. L. Miller, K. D. Kubista, G. M. Rutter, M. Ruan, W. A. de Heer, M. Kindermann, P. N. First, and J. A. Stroscio, *Nature Physics* **6**, 811 (2010).
 - ¹⁶ M. Kindermann and P. N. First, *Phys. Rev. B* **83**, 045425 (2011).
 - ¹⁷ R. Bistritzer and A. H. MacDonald, *PNAS* **108**, 12233 (2011).
 - ¹⁸ M. S. Dresselhaus and G. Dresselhaus, *Advances in Physics* **51**, 1 (2002).
 - ¹⁹ I. Martin, Y. M. Blanter, and A. F. Morpurgo, *Phys. Rev. Lett.* **100**, 036804 (2008).
 - ²⁰ G. W. Semenoff, V. Semenoff, and F. Zhou, *Phys. Rev. Lett.* **101**, 087204 (2008).
 - ²¹ C.-H. Park, L. Yang, Y.-W. Son, M. L. Cohen, and S. G. Louie, *Nature Physics* **4**, 213 (2008).
 - ²² C.-H. Park, Y.-W. Son, L. Yang, M. L. Cohen, and S. G. Louie, *Phys. Rev. Lett.* **103**, 046808 (2009).
 - ²³ L. Brey and H. A. Fertig, *Phys. Rev. Lett.* **103**, 046809 (2009).
 - ²⁴ D. P. Arovas, L. Brey, H. A. Fertig, E.-A. Kim, and K. Ziegler, *arXiv:1002.3655* (2010).
 - ²⁵ J. Goldstone and F. Wilczek, *Phys. Rev. Lett.* **47**, 986 (1981).
 - ²⁶ W. Yao, S. A. Yang, and Q. Niu, *Phys. Rev. Lett.* **102**, 096801 (2009).
 - ²⁷ In the generalization to multilayers the interaction between layers with $j > 0$ needs to be added to the diagonal part $\omega - \sum_j H_j$.